We are IntechOpen, the world's leading publisher of Open Access books Built by scientists, for scientists

4,800
Open access books available

122,000
International authors and editors

135M
Downloads

Our authors are among the

154
Countries delivered to

TOP 1%
most cited scientists

12.2%
Contributors from top 500 universities

CLARIVATE ANALYTICS BOOK CITATION INDEX INDEXED

WEB OF SCIENCE™

Selection of our books indexed in the Book Citation Index in Web of Science™ Core Collection (BKCI)

Interested in publishing with us?
Contact book.department@intechopen.com

Numbers displayed above are based on latest data collected.
For more information visit www.intechopen.com

Chapter 9

Analysis of Energy Harvesting Using Frequency Up-Conversion by Analytic Approximations

Adam Wickenheiser

Additional information is available at the end of the chapter

http://dx.doi.org/10.5772/52075

1. Introduction

Energy harvesting is the process of capturing energy existing in the environment of a wireless device in order to power its electronics without the need to manually recharge the battery. By replenishing on-board energy storage autonomously, the need to recharge or replace the battery can be eliminated altogether, enabling devices to be placed in difficult-to-reach areas. Vibration-based energy harvesting in particular has garnered much attention due to the ubiquity of vibrational energy in the environment, especially around machinery and vehicles (Roundy et al., 2003). Although several methods of electromechanical transduction from vibrations have been investigated, this chapter focuses on utilizing the piezoelectric effect.

Piezoelectric energy harvesters convert mechanical energy into electrical through the strain induced in the material by inertial loads. Typically, piezoelectric material is mounted on a structure that oscillates due to excitation of the host structure to which it is affixed. If a natural frequency of the structure is matched to the predominant excitation frequency, resonance occurs, where large strains in the piezoelectric material are induced by relatively small excitations. In order to take advantage of resonance, the natural frequency of the device must be matched to the predominant frequency component of the base excitation (Anderson & Wickenheiser, 2012). For many potential applications, ambient vibrations are low frequency, requiring longer length scales or a larger mass to match the resonance frequency to the excitation frequency (Roundy et al., 2003; Wickenheiser & Garcia, 2010a; Wickenheiser, 2011). In order to shrink the size and mass of these devices while reducing their natural frequencies, a variety of techniques have been investigated. Varying the cross sections along the beam length (Dietl & Garcia, 2010; Reissman et al., 2007; Roundy et al., 2005) and the ratio of tip mass to beam mass (Dietl & Garcia, 2010; Wickenheiser, 2011) have been shown to improve the electromechanical coupling (a factor in the energy conversion

rate) over a uniform cantilever beam design. Multi-beam structures can reduce the overall dimensions of the design by folding it in on itself while retaining a similar natural frequency to the original, straight configuration (Karami & Inman, 2011; Erturk et al., 2009); however, this requires a more complex analysis of the natural frequencies and mode shapes (Wickenheiser, 2012).

In resonant designs, minimizing the mechanical damping in the system enhances the power harvesting performance (Lefeuvre et al., 2005; Shu and Lien, 2006; Wickenheiser & Garcia, 2010c). Unfortunately, lightly damped systems are the most sensitive to discrepancies between the resonance and the driving frequencies. Several methods have been analyzed for tuning the stiffness of the vibrating beam in order to match a slowly varying base excitation frequency. (Challa et al., 2008) and (Reissman et al., 2009) have considered placing one or more magnets to either side of the tip mass to create either an attractive or repulsive force that changes the effective stiffness of the beam, thus allowing the natural frequencies to be adjusted to match the base excitation frequency. Similarly, (Mann & Sims, 2009) harvest energy from a magnet levitating in a cavity between two magnets; varying the spacing of the magnets changes the natural frequency of the levitation. (Leland & Wright, 2006) have proposed tuning the natural frequencies of the beam by applying an axial load; however, this technique has been found to increase the apparent mechanical damping in the structure. A similar concept has been developed for adjusting the pre-tension in extensional mode resonators (Morris et al., 2008). These methods can be considered "quasi-static" because the rate at which the natural frequencies can be tuned is often much slower than the vibration frequency. Thus, these methods are ideal if the base excitation is an approximately stationary process with frequencies concentrated in a narrow band.

The off-resonant response of these systems can be enhanced by destabilizing the relaxed state of the beam. A bi-stable cantilever beam can be created by adding a repelling magnet beyond a magnetic tip mass or by adding attracting magnets on either side. In this situation, the beam can be induced to jump from one well of attraction to the other either periodically, quasi-periodically, or chaotically, depending on the amplitude and frequency of the base excitation. Bi-stability can be realized with a "snap-through" mechanism, in which the mass moves perpendicularly to the elastic axis (Ramlan et al., 2010), using the aforementioned beam and magnetic set-up first analyzed by (Moon, 1978), and using an inherently bi-stable composite plate (Arrieta, 2010). This technique is suited for strong excitations that are able to drive the beam between the two potential wells; however, for low excitation levels the performance converges towards the linear system unless a perturbation is added to "kick" the system into the other well.

In this chapter, a technique known as frequency up-conversion is employed to generate strong off-resonant responses. This technique is based off a repetition of the bi-stable system to create a sequence of potential wells; the transition between them induces a "pluck" followed by a free response at the fundamental frequency. A similar concept has been pursued by Tieck et al. (2006), consisting of a rack placed transversely near the tip of the

beam that would periodically pluck the beam as it vibrated. Other concepts utilizing mechanical rectification have been proposed for harvesting energy from buoy motion (Murray and Rastegar, 2009) and low-frequency, rotating machinery (Rastegar and Murray, 2008).

In the following sections, the equations of motion (EOMs) are derived for a uniform beam with magnetic tip mass under periodic base excitation. The eigenvalue problem for this design is then solved for the natural frequencies and mode shapes. The modal expansion is reduced to a single mode (the fundamental) in order to derive an approximate model for low frequencies well below the fundamental frequency. A simplification is derived based on neglecting the base excitation; this simplification leads to a model of the beam's excitation in terms of a sequence of plucks followed by free vibrations. A few simple case studies are presented to highlight the accuracy of this approximate model.

2. Derivation of electromechanical EOMs

The layout of the piezoelectric, vibration-based energy harvester and the nearby magnetized structures used for mechanical rectification is presented in Fig. 1. For this study, a bimorph configuration is considered, in which piezoelectric layers are bonded to both sides of an inactive substructure. Other configurations, such as the unimorph, can be modeled with few modifications, as pointed out below. Electrodes are assumed to cover the upper and lower surfaces of each layer, and they are wired together in the "parallel" configuration, as depicted. In this configuration, the voltage drop across each layer is assumed to be the same, and the charge displaced by each layer is additive, much like capacitors in parallel. Because the piezoelectric layers are on opposite sides of the neutral axis, each layer experiences opposite strains; hence, they must be poled in the same direction to avoid charge cancellation. It is assumed that the electrodes and connecting wires have negligible resistance and that the resistivity of the piezoelectric material is significantly higher than that of the external circuitry; thus, the transducer impedance is assumed to be purely reactive.

A tip mass is connected to the free end of the beam, and its center of mass is displaced axially from the connection point by a distance d_t. Tip masses are traditionally added to decrease the natural frequency of the beam and to increase the strain due to base excitation. In this situation, the tip mass is considered to be a permanent magnet and is attracted to ferromagnetic structures placed in a line parallel to the y-axis with spacing d_m between them. These structures are not magnets themselves; rather, they become magnetized due to the proximity of the magnetic tip mass. Thus, in this device, the tip mass is an active component of the excitation while fulfilling its passive role as just described.

In the following section, the EOMs for the electromechanical system presented in Fig. 1 are derived through force, moment, and charge balances while adopting the Euler-Bernoulli beam assumptions and linearized material constitutive equations. The approach taken herein is based on force and moment balances and is a generalization of the treatments by

(Erturk & Inman, 2008; Söderkvist, 1990; Wickenheiser & Garcia, 2010c). It is assumed that each beam segment is uniform in cross section and material properties. Furthermore, the standard Euler-Bernoulli beam assumptions are adopted, including negligible rotary inertia and shear deformation (Inman, 2007). Subsequently, a solution consisting of a series of assumed modes is presented, and the EOMs are decoupled into modal dynamics equations. As will be demonstrated, only the first bending mode is excited significantly by the plucking of the magnetic force. Although higher modes can be excited by higher frequency base excitation, this study focuses primarily on base excitation frequencies well below the fundamental resonant frequency.

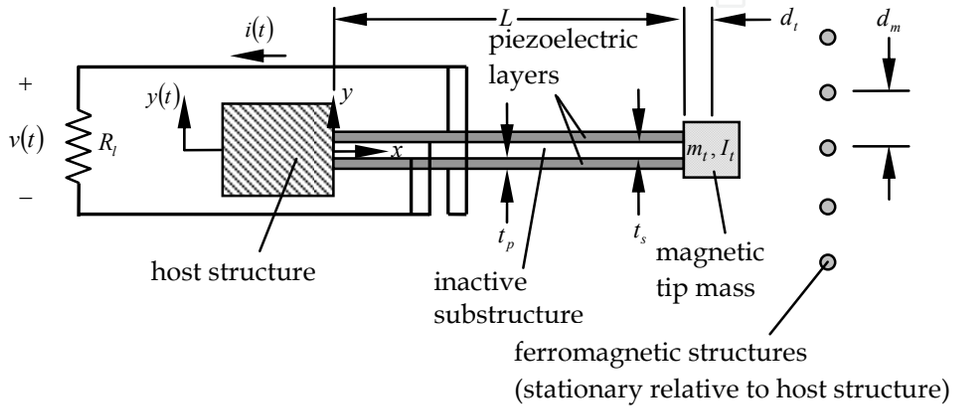

Figure 1. Layout and geometric parameters of cantilevered vibration energy harvester in parallel bimorph configuration with magnetic tip mass

2.1. Electromechanical EOMs

In this derivation, the states of the electromechanical system are the following: $w(x,t)$ is the relative transverse deflection of the beam with respect to its base, $v(t)$ is the voltage across the energy harvester as seen by the external circuit, and $i(t)$ is the net current flowing into the external circuit. The input to the system is $y(t)$, the absolute transverse displacement of the base; therefore, $w(x,t)+y(t)$ is the absolute transverse deflection of the beam.

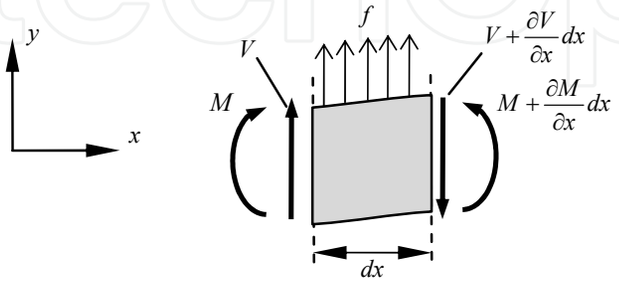

Figure 2. Free-body diagram of Euler-Bernoulli beam segment

Consider the free-body diagram shown in Fig. 2. Dropping higher order terms, balances of forces in the *y*-direction and moments yield

$$\frac{\partial V(x,t)}{\partial x} + f(x,t) = (\rho A)_{eff} \frac{\partial^2 w(x,t)}{\partial t^2} \quad \text{(a)}$$
$$\frac{\partial M(x,t)}{\partial x} = -V(x,t) \quad \text{(b)} \tag{1}$$

where $V(x,t)$ is the shear force, $M(x,t)$ is the internal moment generated by mechanical and electrical strain, $f(x,t)$ is the externally applied force per unit length, and $(\rho A)_{eff}$ is the mass per unit length (Inman, 2007). For the case of a bimorph beam segment, this term is given by

$$(\rho A)_{eff} = \frac{m}{L} = \frac{\rho_s t_s bL + 2\rho_p t_p bL}{L} = b(\rho_s t_s + 2\rho_p t_p) \tag{2}$$

where m is the mass of the beam (not counting the tip mass), L is its length, b is its width, ρ_s and t_s are the density and thickness of the substrate, and ρ_p and t_p are the density and thickness of one of the piezoelectric layers, respectively. As can be seen in Eq. (2), if the segment is monolithic, $(\rho A)_{eff}$ is simply the product of the density of the material and the cross-sectional area. The externally applied force per unit length can be written as the sum of the distributed inertial force along the beam and the inertial force of the tip mass – which arise because the non-inertial frame of the base is taken as the reference – and the magnetic force applied at the center of the tip mass:

$$f(x,t) = -(\rho A)_{eff} \frac{d^2 y(t)}{dt} - m_t \frac{d^2 y(t)}{dt} \delta(x-L) - f_{mag}(t)\delta(x-L) \tag{3}$$

where m_t is the mass of the tip mass, $f_{mag}(t)$ is the magnetic force, and $\delta(\cdot)$ is the Dirac delta function. In this study, the magnetic force is assumed to be purely in the y-direction. Although there is a stiffening effect due to the axial attractive force, it is considered negligible. The negative sign on the magnetic force indicates that it is an attractive force.

The internal bending moment is the net contribution of the stresses in the axial direction in the beam. The stress within the piezoelectric layers is found from the linearized constitutive equations

$$T_1 = c_{11}^E S_1 - e_{31} E_3$$
$$D_3 = e_{31} S_1 + \varepsilon_{33}^S E_3 \tag{4}$$

where T is stress, S is strain, E is electric field, D is electric displacement, c is Young's Modulus, e is piezoelectric constant, and ε is dielectric constant. The subscripts indicate the direction of perturbation; in the cantilever configuration shown in Fig. 1, 1 corresponds to axial and 3 corresponds to transverse. The superscript $(\cdot)^E$ indicates a linearization at constant electric field, and the superscript $(\cdot)^S$ indicates a linearization at constant strain (IEEE, 1987). The use of Eq. (4) assumes the hypothesis of plane stress, which is reasonable since the beams are not directly loaded in the other directions, and small deflections. The

stress within the substrate layer is given simply by the linear stress-strain relationship $T_1 = c_{11,s} S_1$, where $c_{11,s}$ is Young's Modulus of the substrate material in the axial direction. Since deformations are assumed small, the axial strain is the same as the case of pure bending, which is given by $S_1 = -y\partial^2 w(x,t)/\partial x^2$ (Beer & Johnson, 1992), and the transverse electric field is assumed constant and equal to $E_3 = \pm v(t)/t_p$, where $v(t)$ is the voltage across the electrodes, and the top and bottom layer have opposite signs due to the parallel configuration wiring. (This approximation is reasonable given the thinness of the layers.)

Consider the case of a bimorph beam. The bending moment along the length of the beam is

$$\begin{aligned}
M(x,t) &= \int_{-t_s/2-t_p}^{-t_s/2} T_1 b y dy + \int_{-t_s/2}^{t_s/2} T_1 b y dy + \int_{t_s/2}^{t_s/2+t_p} T_1 b y dy \\
&\quad - m_t \frac{d^2 y(t)}{dt} d_t H(x-L) - f_{mag}(t) d_t H(x-L) \\
&= -\left[\int_{-t_s/2-t_p}^{-t_s/2} c_{11}^E b y^2 dy + \int_{-t_s/2}^{t_s/2} c_{11,s} b y^2 dy + \int_{t_s/2}^{t_s/2+t_p} c_{11}^E b y^2 dy \right] \frac{\partial^2 w(x,t)}{\partial x^2} \\
&\quad - \left[\int_{-t_s/2-t_p}^{-t_s/2} \frac{e_{31}}{t_p} b y dy - \int_{t_s/2}^{t_s/2+t_p} \frac{e_{31}}{t_p} b y dy \right] v(t) \left[H(x) - H(x-L) \right] \\
&\quad - m_t \frac{d^2 y(t)}{dt} d_t H(x-L) - f_{mag}(t) d_t H(x-L) \\
&= \underbrace{\left\{ c_{11,s} b \frac{t_s^3}{12} + 2 c_{11}^E b \left[\frac{t_p^3}{12} + t_p \left(\frac{t_p + t_s}{2} \right)^2 \right] \right\}}_{(EI)_{eff}} \frac{\partial^2 w(x,t)}{\partial x^2} \\
&\quad + \underbrace{-e_{31} b (t_s + t_p)}_{\vartheta} v(t) \left[H(x) - H(x-L) \right] \\
&\quad - m_t \frac{d^2 y(t)}{dt} d_t H(x-L) - f_{mag}(t) d_t H(x-L)
\end{aligned} \tag{5}$$

where $H(\cdot)$ is the Heaviside step function. In Eq. (5), the constant multiplying the $\partial^2 w(x,t)/\partial x^2$ term is defined as $(EI)_{eff}$, the effective bending stiffness. (Note that if the beam segment is monolithic, this constant is simply the product of the Young's Modulus and the moment of inertia.) The constant multiplying the $v(t)$ term is defined as ϑ, the electromechanical coupling coefficient. Substituting Eq. (5) into Eq. (1) yields

$$\begin{aligned}
&(\rho A)_{eff} \frac{\partial^2 w(x,t)}{\partial t^2} + (EI)_{eff} \frac{\partial^4 w(x,t)}{\partial x^4} + \vartheta \left[\frac{d\delta(x)}{dx} - \frac{d\delta(x-L)}{dx} \right] v(t) = \\
&-(\rho A)_{eff} \frac{d^2 y(t)}{dt} - \left[m_t \frac{d^2 y(t)}{dt} + f_{mag}(t) \right] \left[\delta(x-L) + d_t \frac{d\delta(x-L)}{dx} \right]
\end{aligned} \tag{6}$$

which is the transverse mechanical EOM for the beam.

The electrical EOM can be found by integrating the electric displacement over the surface of the electrodes, yielding the net charge $q(t)$ (IEEE, 1987):

$$\begin{aligned} q(t) &= \iint_{\substack{\text{upper}\\\text{layer}}} D_3 dA - \iint_{\substack{\text{lower}\\\text{layer}}} D_3 dA \\ &= b\int_0^L \left[\frac{1}{t_p}\int_{t_s/2}^{t_s/2+t_p} -e_{31} y \frac{\partial^2 w(x,t)}{\partial x^2} dy - \frac{\varepsilon_{33}^S}{t_p} v(t) \right] dx \\ &\quad -b\int_0^L \left[\frac{1}{t_p}\int_{-t_s/2-t_p}^{-t_s/2} -e_{31} y \frac{\partial^2 w(x,t)}{\partial x^2} dy + \frac{\varepsilon_{33}^S}{t_p} v(t) \right] dx \\ &= \underbrace{-e_{31} b (t_s + t_p)}_{\vartheta} \left. \frac{\partial w(x,t)}{\partial x} \right|_{x=L} - \underbrace{\frac{2\varepsilon_{33}^S bL}{t_p}}_{C_0} v(t) \end{aligned} \tag{7}$$

where the constant multiplying the $v(t)$ term is defined as C_0, the net clamped capacitance of the segment. Eqs. (6–7) provide a coupled system of equations; these can be solved by relating the voltage $v(t)$ to the charge $q(t)$ through the external electronic interface.

2.2. Modal decoupling

The system of coupled equations (6–7) can be solved by assuming that the transverse deflection of the beam can be written as a convergent series expansion of eigenfunctions, i.e.

$$w(x,t) = \sum_{i=1}^{\infty} \phi_i(x) \eta_i(t) \tag{8}$$

where $\phi_i(x)$ is the i^{th} transverse mode shape function, and $\eta_i(t)$ is the i^{th} modal displacement. Given the configuration in Fig. 1 with a tip mass having a nontrivial mass m_t and moment of inertia I_t, the eigenvalues λ_i corresponding to the mode shapes must satisfy

$$F_{cf} - \frac{m_t}{(\rho A)_{eff} L} \lambda F_{cp} - \frac{I_t + m_t d_t^2}{(\rho A)_{eff} L^3} \lambda^3 F_{cr} + \frac{I_t m_t}{(\rho A)_{eff}^2 L^4} \lambda^4 F_{cc} - \frac{2 m_t d_t}{(\rho A)_{eff} L^2} \lambda^2 \sin\lambda \sinh\lambda = 0 \tag{9}$$

where $F_{cf} = 1 + \cos\lambda \cosh\lambda$ are the clamped-free, $F_{cp} = \sin\lambda \cosh\lambda - \cos\lambda \sinh\lambda$ are the clamped-pinned, $F_{cr} = \sin\lambda \cosh\lambda + \cos\lambda \sinh\lambda$ are the clamped-rolling, and $F_{cc} = 1 - \cos\lambda \cosh\lambda$ are the clamped-clamped eigenvalue terms, respectively (Oguamanam, 2003). The mode shape functions are given by

$$\phi_i(x) = \cos\left(\lambda_i \frac{x}{L}\right) - \cosh\left(\lambda_i \frac{x}{L}\right) + \frac{\sin\lambda_i - \sinh\lambda_i - \frac{m_t}{(\rho A)_{eff} L}\left[\lambda_i^2 \frac{d_t}{L}(\sin\lambda_i + \sinh\lambda_i) - \lambda_i(\cos\lambda_i - \cosh\lambda_i)\right]}{\cos\lambda_i + \cosh\lambda_i - \frac{m_t}{(\rho A)_{eff} L}\left[\lambda_i^2 \frac{d_t}{L}(\cos\lambda_i - \cosh\lambda_i) + \lambda_i(\sin\lambda_i - \sinh\lambda_i)\right]} \times\left[\sin\left(\lambda_i \frac{x}{L}\right) - \sinh\left(\lambda_i \frac{x}{L}\right)\right] \tag{10}$$

These functions may be scaled arbitrarily and still be admissible, and in the present case are done to satisfy the following orthogonality condition:

$$\int_0^L (\rho A)_{eff}\, \phi_i(x)\phi_j(x)dx + m_t\phi_i(L)\phi_j(L) + m_t d_t\left[\frac{d\phi_i(x)}{dx}\phi_j(x) + \phi_i(x)\frac{d\phi_j(x)}{dx}\right]_{x=L} + \left(I_t + m_t d_t^2\right)\left[\frac{d\phi_i(x)}{dx}\frac{d\phi_j(x)}{dx}\right]_{x=L} = \delta_{ij} \tag{11}$$

where δ_{ij} is the Kronecker delta.

Substituting (8) into (6) and applying the orthogonality condition (11) results in

$$\frac{d^2\eta_k(t)}{dt^2} + 2\zeta_k\omega_k\frac{d\eta_k(t)}{dt} + \omega_k^2\eta_k(t) + \Theta_k v(t) = -(\rho A)_{eff}\,\gamma_k\frac{d^2y(t)}{dt^2} - \beta_k\left[m_t\frac{d^2y(t)}{dt} + f_{mag}(t)\right] \tag{12}$$

at which point a modal damping term has been inserted. The k^{th} modal short-circuit (i.e. $v(t) = 0$) natural frequency ω_k is given by

$$\omega_k = \sqrt{\frac{\lambda_k^4 (EI)_{eff}}{(\rho A)_{eff} L^4}} \tag{13}$$

for Euler-Bernoulli beams. Eq. (12) constitutes the EOM for the k^{th} transverse vibrational mode. The modal influence coefficients appearing in Eq. (12) are given by

$$\Theta_k = \vartheta\left.\frac{d\phi_k(x)}{dx}\right|_{x=L},\ \gamma_k = \int_0^L \phi_k(x)dx,\ \beta_k = \phi_k(L) + d_t\left.\frac{d\phi_k(x)}{dx}\right|_{x=L} \tag{14}$$

Θ_k is the modal electromechanical coupling coefficient, γ_k is the modal influence coefficient of the distributed inertial force along the beam, and β_k is the modal influence

coefficient of the concentrated force at the tip. A similar decoupling of the electrical EOM (7) yields

$$q(t) = \sum_{i=1}^{\infty} \Theta_i r_i(t) - C_0 v(t) \tag{15}$$

It remains to write the applied magnetic force $f_{mag}(t)$ in terms of the modal coordinates. Due to the assumption of a symmetrical tip mass, this force is applied at its centroid, as shown in Fig. 3. It is further assumed that the ferromagnetic structures are placed uniformly with spacing d_m and that distant structures do not influence the magnetic force (a reasonable assumption given the $1/r^3$ dependency). Additionally, the rotation of the tip mass is assumed small compared to its absolute translation (base motion + relative deflection), and so its effect on the magnitude of the magnetic force is ignored. Thus, the magnetic force is approximately sinusoidal with wavelength d_m, and so it can be written in the form

$$f_{mag}(t) = F_{mag} \sin\left[\frac{2\pi}{d_m}\left(w(x_m, t) + y(t)\right)\right] \tag{16}$$

where x_m is the x-coordinate of the tip mass centroid. The magnitude of this force F_{mag} is a complicated function of the material properties and geometry of the tip mass and the ferromagnetic structures that is beyond the scope of this work (see Moon, 1978; Stanton et al., 2010). F_{mag} is normalized by the maximum static tip load the beam can support without failing. In this study, a maximum strain of 0.1% is chosen, resulting in a maximum static tip load of

$$F_{\max} = \frac{(EI)_{eff}}{\left(\frac{t_s}{2} + t_p\right)L}(0.001) \tag{17}$$

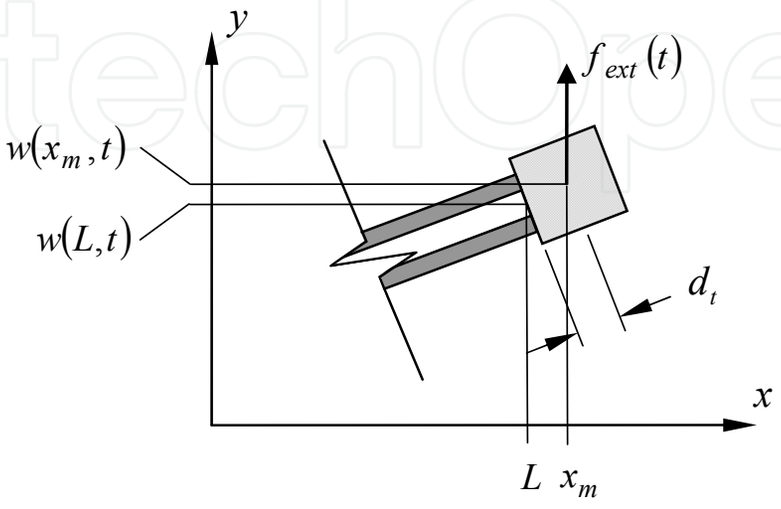

Figure 3. Tip mass coordinates used for locating the centroid in terms of modal coordinates.

The position of the tip mass centroid, shown in Fig. 3, can be written in terms of the modal coordinates:

$$w\left(x_m,t\right)\approx w\left(L,t\right)+d_t\left.\frac{\partial w\left(x,t\right)}{\partial x}\right|_{x=L}=\sum_{i=1}^{\infty}\beta_i\eta_i\left(t\right) \tag{18}$$

3. Estimates of expected power harvested

3.1. Linear case, frequency domain

In order to establish a baseline against which the effects of the magnetic force can be compared, in this section the magnetic interactions are not considered, i.e. $F_{mag}=0$. The most prevalent (e.g. duToit et al., 2005; Lefeuvre et al., 2005; Liao & Sodano, 2008; Shu & Lien, 2006) assumption of constant-amplitude, sinusoidal base excitation forms the basis for analysis of more complex periodic forcing. In this study, it is assumed that the base acceleration is a weakly stationary random process. This general framework includes the special cases of harmonic (single or multiple frequencies), white noise, band-limited noise, and periodic in mean square processes (Anderson & Wickenheiser, 2012; Lin, 1967). The average power dissipated by the load after transients have died out is given by

$$E\left[P\left(t\to\infty\right)\right]=\frac{E\left[v^2\left(t\to\infty\right)\right]}{R_l}=\frac{R_{vv}\left(0\right)}{R_l}=\frac{1}{R_l}\int_{-\infty}^{\infty}\left|H\left(\omega\right)\right|^2\Phi_{AA}\left(\omega\right)d\omega \tag{19}$$

where $E\left[\cdot\right]$ is the expectation operator, $R_{vv}\left(\tau\right)$ is the autocorrelation function of the voltage, $H\left(\omega\right)$ is the frequency transfer function of the energy harvester between acceleration and voltage, and $\Phi_{AA}\left(\omega\right)$ is the spectral density of the base acceleration (Lin, 1967). Since the system is assumed to be stable, the power output is seen to approach a weakly stationary process as $t\to\infty$.

In order to calculate the frequency transfer function, it is assumed that the electrical load can be represented by a resistor with value R_l. Eq. (15) can then be rewritten as

$$\frac{v\left(t\right)}{R_l}=i\left(t\right)=\frac{dq\left(t\right)}{dt}=\sum_{i=1}^{\infty}\Theta_i\frac{d\eta_i\left(t\right)}{dt}-C_0\frac{dv\left(t\right)}{dt} \tag{20}$$

Since the system of equations (12,19) is linear, the modal responses $\eta_k\left(t\right)$ and output voltage $v\left(t\right)$ are sinusoidal at the driving frequency of the base excitation. The frequency transfer function between base displacement and voltage can be derived from the EOMs, yielding

$$\frac{V\left(\omega\right)}{Y\left(\omega\right)}=\frac{R_l\sum_{j=1}^{\infty}\Theta_j^2\frac{i\left[\left(\rho A\right)_{eff}\gamma_j+m_t\beta_j\right]\omega^3}{\omega_j^2-\omega^2+i2\zeta_j\omega_j\omega}}{iR_lC_0\omega+1+R_l\sum_{j=1}^{\infty}\Theta_j^2\frac{i\omega}{\omega_j^2-\omega^2+i2\zeta_j\omega_j\omega}} \tag{21}$$

where $i=\sqrt{-1}$ and ω is the base excitation frequency (Wickenheiser & Garcia, 2010b). The frequency transfer function between base acceleration and displacement is simply $Y(\omega)/A(\omega)=-1/\omega^2$. In this study, however, only the fundamental mode is assumed to be excited; hence, the j subscript is dropped and the fundamental natural frequency is written as ω_n.

In order to use Eq. (18), an estimate of the spectral density of the base acceleration $\Phi_{AA}(\omega)$ is required. An overview of spectral density estimation methods can be found in (Porat, 1994), any of which can provide an approximation of the base excitation signal of the form

$$\frac{d^2y(t)}{dt^2}\equiv a(t)\approx\sum_{k=1}^{N}A_k\cos(\omega_k t+\varphi_k) \tag{22}$$

where the component amplitudes A_k, frequencies ω_k, and phase angles φ_k are obtained from the spectral density estimate. The number of terms needed N is often determined by a user-defined error tolerance used to capture the "quality" of the signal approximation in some optimal manner. The spectral density is then given by

$$\begin{aligned}\Phi_{AA}(\omega)&=\frac{1}{2\pi}\int_{-\infty}^{\infty}R_{AA}(t)e^{-i\omega t}dt=\frac{1}{2\pi}\int_{-\infty}^{\infty}E\left[a(t_0+t)\overline{a(t_0)}\right]e^{-i\omega t}dt\\&=\frac{1}{2\pi}\int_{-\infty}^{\infty}\lim_{T\to\infty}\frac{1}{T}\int_0^T\left[a(t_0+t)\overline{a(t_0)}\right]dt_0e^{-i\omega t}dt\end{aligned} \tag{23}$$

Consider first the case $N=2$, where the base excitation is composed of the sum of two sinusoids. Then, without loss of generality,

$$a(t)=\underbrace{A_1\cos(\omega_1 t)}_{a_1(t)}+\underbrace{A_2\cos(\omega_2 t+\varphi)}_{a_2(t)}=\frac{A_1}{2}\left(e^{i\omega_1 t}+e^{-i\omega_1 t}\right)+\frac{A_2}{2}\left(e^{i(\omega_2 t+\varphi)}+e^{-i(\omega_2 t+\varphi)}\right) \tag{24}$$

Then

$$\begin{aligned}R_{AA}(t)=R_{A_1A_1}(t)+R_{A_2A_2}(t)+\frac{A_1A_2}{4}\lim_{T\to\infty}\frac{1}{T}\int_0^T\left(e^{i\left[\omega_2(t_0+t)+\varphi\right]}+e^{-i\left[\omega_2(t_0+t)+\varphi\right]}\right)\left(e^{-i\omega_1 t_0}+e^{i\omega_1 t_0}\right)dt_0\\+\frac{A_1A_2}{4}\lim_{T\to\infty}\frac{1}{T}\int_0^T\left(e^{i\omega_1(t_0+t)}+e^{-i\omega_1(t_0+t)}\right)\left(e^{-i(\omega_2 t_0+\varphi)}+e^{i(\omega_2 t_0+\varphi)}\right)dt_0\end{aligned} \tag{25}$$

Integrating the first term in the integrand and taking the limit yields

$$\begin{aligned}\lim_{T\to\infty}\frac{1}{T}\int_0^T e^{i\left[\omega_2(t_0+t)+\varphi\right]}e^{-i\omega_1 t_0}dt_0&=\lim_{T\to\infty}\frac{1}{T}\frac{1}{i(\omega_2-\omega_1)}\left(e^{i\left[(\omega_2-\omega_1)T+\omega_2 t+\varphi\right]}-e^{i(\omega_2 t+\varphi)}\right)\\&\le\lim_{T\to\infty}\frac{1}{T}\frac{1}{|\omega_2-\omega_1|}(1+1)=0\end{aligned} \tag{26}$$

Each of the other integrated terms also averages out to 0 in the long run; hence,

$$R_{AA}(t) = R_{A_1A_1}(t) + R_{A_2A_2}(t) \tag{27}$$

Then, by mathematical induction,

$$R_{AA}(t) = \sum_{k=1}^{N} R_{A_kA_k}(t) \tag{28}$$

Using this result in Eq. (23) gives

$$\begin{aligned}\Phi_{AA}(\omega) &= \frac{1}{2\pi}\int_{-\infty}^{\infty} R_{AA}(t)e^{-i\omega t}dt = \frac{1}{2\pi}\int_{-\infty}^{\infty} e^{-i\omega t}\sum_{k=1}^{N}\frac{A_k^2}{4}\left(e^{i\omega_k t} + e^{-i\omega_k t}\right)dt \\ &= \sum_{k=1}^{N}\frac{A_k^2}{4}\left[\delta(\omega-\omega_k) + \delta(\omega+\omega_k)\right]\end{aligned} \tag{29}$$

Using Eqs. (19,29), the average power harvested can be simplified:

$$E\left[P(t\to\infty)\right] = \frac{1}{2R_l}\sum_{k=1}^{N}\frac{A_k^2}{\omega_k^4}\left|H(\omega_k)\right|^2 \tag{30}$$

Eq. (30) indicates that the frequency transfer function $H(\omega)$ need only be evaluated at the component frequencies of the base acceleration. This equation can be rewritten in the form

$$E\left[P(t\to\infty)\right] = \sum_{k=1}^{N} A_k^2 C_k \tag{31}$$

where C_k can be interpreted as the gain of the harmonic of frequency ω_k. This gain is given by the formula

$$C_k = \frac{\left[(\rho A)_{eff}\gamma + m_t\beta\right]^2 \alpha k_e^2}{2\omega_n}\frac{\Omega_k^2}{\Lambda_k(i\Omega_k)\overline{\Lambda_k(i\Omega_k)}} \tag{32}$$

where

$$\Lambda_k(i\Omega_k) = \alpha(i\Omega_k)^3 + (2\zeta\alpha+1)(i\Omega_k)^2 + (\alpha+2\zeta+\alpha k_e^2)(i\Omega_k) + 1 \tag{33}$$

The following non-dimensional parameters are employed in Eqs. (32-33):

$$\Omega_k = \frac{\omega_k}{\omega_n},\ k_e^2 = \frac{\Theta^2}{C_0\omega_n^2},\ \alpha = R_lC_0\omega_n \tag{34}$$

where Ω_k is the ratio of the frequency of the acceleration component to the fundamental natural frequency, k_e^2 is the modal electromechanical coupling coefficient, and α is the ratio of the load resistance to the modal impedance.

3.2. Nonlinear case, time domain

In the presence of the magnetic field, the EOMs become nonlinear, and the analysis based off of the frequency transfer function detailed in the previous section is no longer valid. Instead, the vibrations induced by the spatially periodic magnetic field are interpreted as a series of plucks that occur each time the tip mass crosses an unstable equilibrium point between the ferrous structures. Each pluck is followed by a free response – underdamped in this case – superposed on the relatively slow base motion. An example response showing these two superposed motions is depicted in Fig. 4. The free response at the fundamental frequency of the beam, as opposed to the frequency of the base motion, drives the majority of the energy harvested.

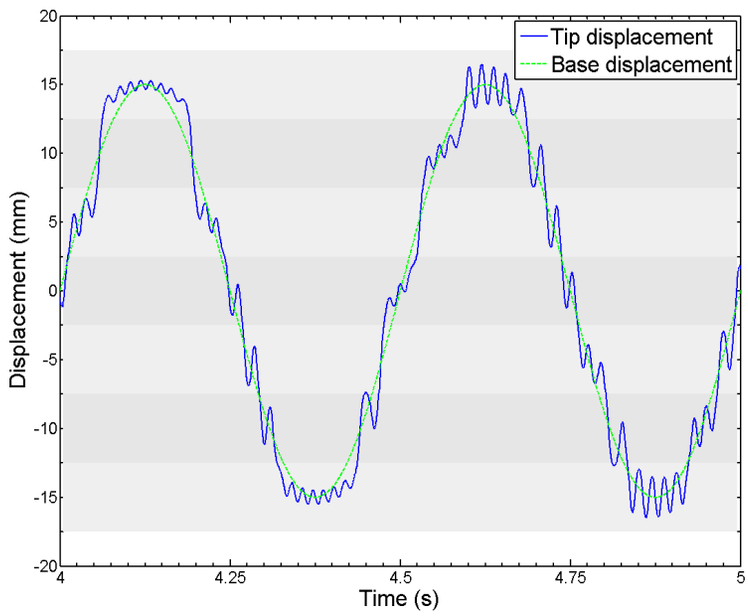

Figure 4. Absolute base and tip displacements: $F_{mag} = 0.75F_{\max}$, $d_m = 5$ mm, $y(t) = Y\sin(\omega t)$, $Y = 15$ mm, $\omega = 2$ Hz. The shaded areas are the basins of attraction of the stable equilibria (Wickenheiser & Garcia, 2010b).

To analyze the energy harvested from a pluck, first the effect of the magnetic field strength on the free response is considered. To simplify the analysis, the inertial force due to base excitation is assumed to be negligible, and the effect of the energy dissipated by the resistor is approximated by an additional damping term. Hence, the total effective modal damping ratio is written as $\zeta_{eff} = \zeta + \zeta_e$, the sum of the mechanical and electrical damping. The electrical damping term can be accurately approximated as

$$\zeta_e = \frac{k_e^2}{2\sqrt{1-k_e^2}} \frac{\alpha}{1+\alpha^2} \tag{35}$$

in the case of steady-state oscillations (Davis & Lesieutre, 1995); this formula is validated for free oscillations in the sequel. Using this damping model, the modal EOM, Eq. (12), can be written as

$$\frac{d^2\eta(t)}{dt^2} + 2\zeta_{eff}\omega_n \frac{d\eta(t)}{dt} + \omega_n^2\eta(t) = -F_{mag}\beta \sin\left[\frac{2\pi}{d_m}\left(\beta\eta(t) + y(t)\right)\right] \tag{36}$$

Linearizing Eq. (36) about the point $y(t) = kd_m$, $\eta(t) = 0$, where k is an integer, gives

$$\frac{d^2\eta(t)}{dt^2} + 2\zeta_{eff}\omega_n \frac{d\eta(t)}{dt} + \left(\omega_n^2 + \frac{2\pi\beta^2}{d_m}F_{mag}\right)\eta(t) = 0 \tag{36a}$$

Thus, the term in parentheses is the square of the effective natural frequency, $\omega_{n,eff}^2$.

The amplitude of each pluck, and hence, the initial condition of the free response, is determined by the location of the unstable equilibrium between each pair of ferrous structures. In equilibrium,

$$\omega_n^2\eta(t) = -F_{mag}\beta \sin\left[\frac{2\pi}{d_m}\left(\beta\eta(t) + y(t)\right)\right] \tag{37}$$

again assuming that the effect of the electromechanical coupling is negligible. First, consider the case when the base is moving upward, i.e. $\dot{y}(t) > 0$. In this case, the pluck occurs when

$$\sin\left[\frac{2\pi}{d_m}\left(\beta\eta(t) + y(t)\right)\right] = 1 \tag{38}$$

When this condition occurs, any more vertical motion of the tip results in a decreased downward magnetic force. At this point, the beam has passed over a local maximum in the magnetic potential, and it begins accelerating towards the next stable equilibrium. The response after cresting the potential hill is approximated by Eq. (36). By plugging Eq. (38) into Eq. (37), the amplitude of the pluck can be found:

$$\eta_0 = \frac{-F_{mag}\beta}{\omega_n^2} \tag{39}$$

If the times of the plucks are denoted t_k, then solving Eq. (38) for t_k, and using the fact that $y(t_k) = Y\sin(\omega t_k)$, yields

$$t_k = \frac{1}{\omega}\sin^{-1}\left(\frac{4k-3}{4}\frac{d_m}{Y} + \frac{F_{mag}\beta^2}{\omega_n^2 Y}\right),\ k = 1,\ldots,N \text{ where } (N-1)d_m < Y \le Nd_m \tag{40}$$

A similar formula can be derived for the pluck times when $\dot{y}(t) < 0$:

$$t_{k+N} = \frac{\pi}{\omega} - \frac{1}{\omega}\sin^{-1}\left(\frac{4(N-k+1)-1}{4}\frac{d_m}{Y} - \frac{F_{mag}\beta^2}{\omega_n^2 Y}\right),\ k = 1,\ldots,N \tag{41}$$

By examining Eq. (36), the (in this case) underdamped free response can be found to be

$$\eta(t) = \eta_0 e^{-\zeta_{eff}\omega_{n,eff}t}\cos\left(\omega_{d,eff}t\right) \tag{42}$$

where $\omega_{d,eff} = \omega_{n,eff}\sqrt{1-\zeta_{eff}^2}$ is the effective damped natural frequency, and the initial amplitude η_0 is given by Eq. (39). This solution can now be plugged into Eq. (20) to find the voltage response $v(t)$ after the pluck. Assuming that the voltage is 0 at the time of the pluck, the solution is given by

$$v(t) = -X_1 e^{-t/R_l C_0} + X_1 e^{-\zeta_{eff}\omega_{n,eff}t}\cos\left(\omega_{d,eff}t\right) + X_2 e^{-\zeta_{eff}\omega_{n,eff}t}\sin\left(\omega_{d,eff}t\right) \tag{43}$$

where

$$X_1 = \frac{\left(\Omega_{eff}\alpha\right)^2 - \zeta_{eff}\Omega_{eff}\alpha}{1-2\zeta_{eff}\Omega_{eff}\alpha+\left(\Omega_{eff}\alpha\right)^2}\frac{\Theta}{C_0}\eta_0,\ X_2 = \frac{\zeta_{eff}\left(\Omega_{eff}\alpha\right)^2 - \left(\Omega_{eff}\alpha\right)^2 - \Omega_{eff}\alpha}{1-2\zeta_{eff}\Omega_{eff}\alpha+\left(\Omega_{eff}\alpha\right)^2}\sqrt{1-\zeta_{eff}^2}\frac{\Theta}{C_0}\eta_0,$$

and $\Omega_{eff} = \omega_{n,eff}/\omega_n$.

The energy harvested during the free vibrations can be adequately approximated by the following formula:

$$\begin{aligned} E(t) &= \frac{1}{R_l}\int_0^t v^2(\tau)d\tau \approx \frac{1}{2R_l}\int_0^t \frac{\Theta^2 R_l^2\omega_{n,eff}^2}{1-2\zeta_{eff}\Omega_{eff}\alpha+\left(\Omega_{eff}\alpha\right)^2}\eta_0^2 e^{-2\zeta_{eff}\omega_{n,eff}\tau}d\tau \\ &= \frac{\Theta^2 R_l\omega_{n,eff}}{4\zeta_{eff}-8\zeta_{eff}^2\Omega_{eff}\alpha+4\zeta_{eff}\left(\Omega_{eff}\alpha\right)^2}\eta_0^2\left(1-e^{-2\zeta_{eff}\omega_{n,eff}\tau}\right) \end{aligned} \tag{44}$$

The accuracy of this approximate formula can be seen in Fig. 5. The results of the simulation of the original EOMs, Eqs. (12,20), are plotted using a solid line, whereas Eq. (44) is plotted using a dashed line. To arrive at Eq. (44), it is assumed that the initial transients and the oscillating terms in $v^2(t)$ integrate out to 0; hence, the result is a smooth exponential curve. Although instantaneously the approximate curve may not be accurate, it matches the overall growth of the exact solution. Hence, Eq. (44) is an accurate representation of the energy harvested from a free vibration with a non-zero initial deflection and a zero initial velocity.

For a sequence of plucks, which is what occurs with the frequency up-conversion technique, it is assumed that the plucks are instantaneous and that the deflection is "reset" to the value given by Eq. (39) after each pluck. Hence, the total energy harvested during a half cycle of the base excitation is

$$E_{total} = \sum_{k=1}^{N} E\left(t_{k+1} - t_k\right) \tag{45}$$

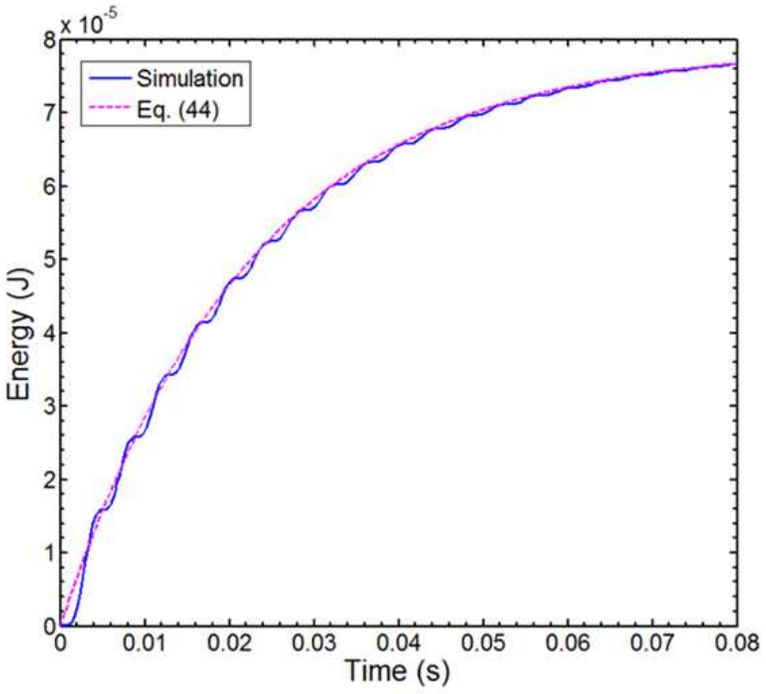

Figure 5. Energy harvested during one free vibration after an initial pluck, comparison between simulation using exact EOMs and approximation using Eq. (44). Parameters used are listed in Table 1.

4. Simulated response to sinusoidal base excitation

In this section, the response of the system to sinusoidal base excitation, $y(t) = Y \sin(\omega t)$, is presented in both the time and frequency domains. The geometry and material properties used in the following simulations are listed in Table 1. The tip mass m_t is approximately one-third of the overall beam mass, and its moment of inertia I_t is calculated assuming the mass is roughly cube-shaped. The resistor value chosen for this study is the optimal value for energy harvesting at the fundamental frequency in the limit of small electromechanical coupling, i.e. $R = 1/(C_0 \omega_{SC,1})$ (Wickenheiser & Garcia, 2010c).

The first three natural frequencies of the beam are $\omega_{SC,1} = 34.1$ Hz, $\omega_{SC,2} = 271.6$ Hz, and $\omega_{SC,3} = 806.8$ Hz. Since frequencies around and below the fundamental frequency are of interest in this study, a three-mode expansion of the beam displacement is deemed sufficient. Furthermore, since the magnetic force is applied at the tip of the beam, only the fundamental mode is significantly excited by the plucking.

The transfer functions for power harvested (normalized by $Y^2\omega^3$) are plotted in Fig. 6. Five different values for the magnetic force strength F_{mag} are plotted alongside the baseline case of an inactive tip. For the cases with a nonzero magnetic force, the transfer functions are derived numerically. The system is simulated for 50 cycles of base motion, and the relative tip deflection is averaged over the last 20 cycles of each run in order to minimize the effects of initial transients. This process is completed 10 times at every frequency, and the results are averaged.

Beam properties:		
L	length	100 mm
b	width	20 mm
t_s	thickness of substructure	0.5 mm
t_p	thickness of PZT layer	0.4 mm
ρ_s	density of substructure	7800 kg/m^3
ρ_p	density of PZT	7800 kg/m^3
$c_{11,s}$	Young's modulus of substructure	102 GPa
c_{11}^E	Young's modulus of PZT	66 GPa
e_{31}	piezoelectric constant	-12.54 C/m^2
ε_{33}^S	permittivity	15.93 nF/m
ζ	modal damping ratio	6.4%
Tip mass properties:		
m_t	mass	10 g
d_t	centroid displacement	5 mm
I_t	moment of inertia	1.7x10^{-7} kg–m^2
Derived properties:		
$(\rho A)_{eff}$	mass per length	0.20 kg/m
$(EI)_{eff}$	bending stiffness	0.25 N–m^2
C_0	net clamped capacitance	160 nF
k_e^2	electromechanical coupling coefficient	0.049
R	resistance	29.3 kΩ

Table 1. Geometry and material properties.

The overall trend of the responses indicates that the magnet has an increasing effect as the base excitation frequency decreases to 0. As is discussed in the sequel, at low frequencies relative to the fundamental resonance, the response converges to a sequence of free responses. In this regime, the inertial forces are negligible, and so the disturbances due to the magnetic force are relatively large. The normalized power approaches half an order of magnitude below its resonance value as $\omega \to 0$ due to the energy harvested from the plucks. As the driving frequency increases, the beam tip has less time to oscillate in each potential well, and, thus, its motion tends to converge towards the motion of the baseline case. As $\omega \to \omega_{SC,1}$, the frequency of the base motion approaches the frequency of the impulse response of the beam from the magnetic force. Hence, the time in which the beam is in free response decays to 0, and so all of the frequency response functions converge towards the baseline function, as shown in Fig. 5. A discussion of the variation in frequency response with respect to the magnet parameters F_{mag} and d_m can be found in (Wickenheiser & Garcia, 2010b).

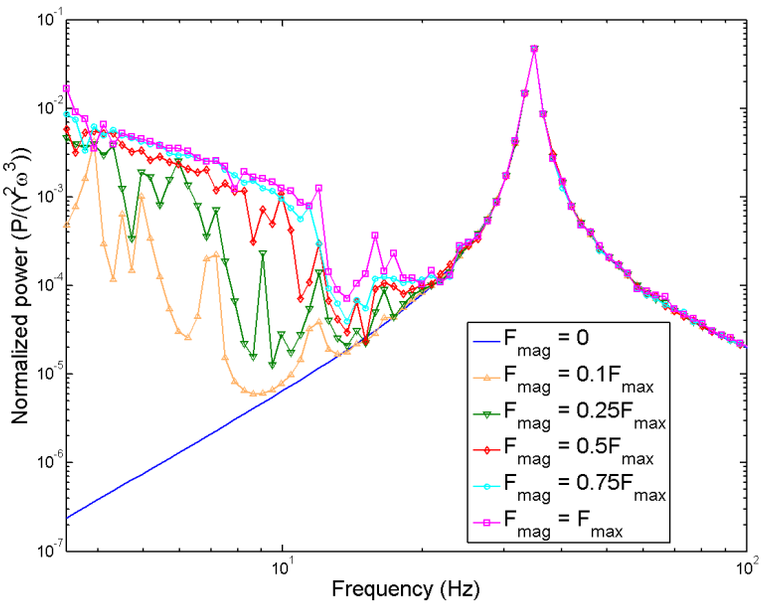

Figure 6. Normalized power harvested transfer function: $d_m = 5$ mm, $Y = 15$ mm (Wickenheiser & Garcia, 2010b).

Fig. 7 compares two methods of simulating the tip deflection response: using the original EOMs and assuming a series of undamped free responses give by Eq. (42). The most notable difference that can be seen from the figure is that the free response assumption does not take into account the base motion, which causes the solution to the EOMs to drift upward or downward depending on the sign of the base velocity. Another difference between the two models is that the assumed time of the plucks, indicated by the vertical lines and given by Eqs. (40,41), generally occur before the plucks in the actual solution. This happens because the beam has enough inertia to resist the pull of the next magnet, i.e. to overcome the potential well barrier between magnets. Only after the beam's velocity decays sufficiently does it become trapped in the next potential well in the sequence.

Fig. 8 depicts the voltage response during the same simulation that has been plotted in Fig. 7. A comparison of the two curves plotted shows an excellent agreement between the simulation results and the predicted voltage given by Eq. (43). There is a slight asymmetry in the curve representing the simulation results due to the base excitation. This discrepancy is much less pronounced than in Fig. 7 since the voltage is dominated by the velocity of the tip deflection, which is not affected directly by the base motion, unlike the tip position. The primary difference between the two curves in Fig. 8 is the error in predicting when the plucks occur, as discussed in the previous paragraph. This error causes an over-prediction in the number of cycles of free oscillation, but this error is small compared to the duration of the free response between plucks. The initial magnitude of the voltage free response is well predicted, however; this prediction is much more significant in the estimation of voltage given by Eq. (43).

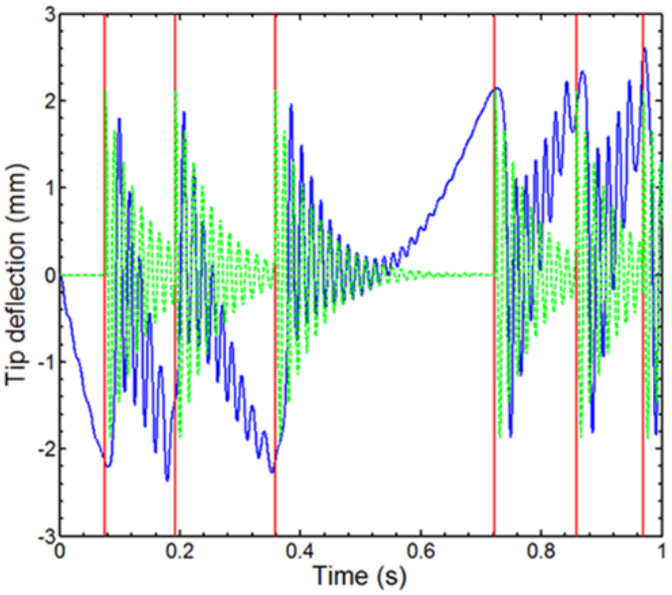

Figure 7. Comparison of simulated tip deflection from EOMs (solid) and a series of plucks, Eq. (42) (dashed). Vertical lines indicate the estimated times of plucking according to Eqs. (40,41).

Fig. 9 shows the comparison between the power frequency transfer functions of the simulation, the approximation by a series of plucks, and the linear system (without magnets). This plot is generated using the same procedure as the one used to produce Fig. 6. The most striking feature of this plot is that the simulation results are seen to converge to the approximation by a series of plucks for low frequencies and converge to the linear system approximation at frequencies approaching the fundamental resonance. As previously mentioned, at frequencies around the fundamental resonance, the beam is not allowed to vibrate freely because the pluck frequency exceeds its natural frequency. Hence, there is no exponential decay in the amplitude of the tip deflection between plucks. In this case, the forced response (i.e. particular solution) dominates the motion, and so the frequency transfer function of the nonlinear system approaches that of the linear system. At low frequencies, the base excitation term becomes negligible, and so the mechanical EOM

reduces to Eq. (36), the basis for the series of plucks approximation. In this scenario, the magnetic force drives the excitation of the beam, whereas the inertial force due to the base excitation is negligible. This is manifested in the decrease in the linear response at low frequencies.

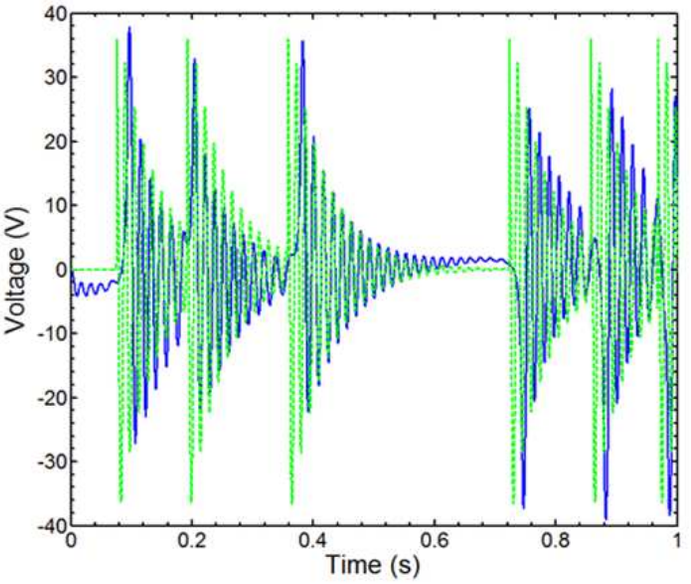

Figure 8. Comparison of simulated voltage from EOMs (solid) and a series of plucks, Eq. (43) (dashed).

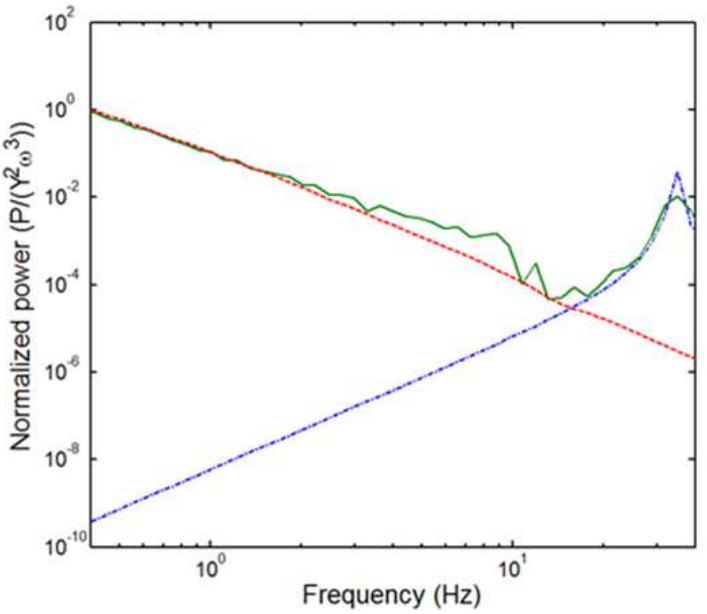

Figure 9. Comparisons of normalized power frequency transfer functions between EOMs (solid), a series of plucks (dashed), and the linear system (dash-dot).

5. Conclusions

This chapter presents an accurate means of approximating the non-linear response of the frequency up-conversion technique as a series of free responses. This simplification is based

on the assumption that the base excitation is negligible, and so it only holds at low frequencies compared to the fundamental resonance of the beam. This approximation, however, is useful in the design of energy harvesters utilizing this technique as it enables power to be generated at very low frequencies. This means that the device can be designed for a fundamental frequency much higher than the nominal base excitation frequency, which tends to result in smaller and lighter transducers. At low frequencies, the approximation derived herein is shown to agree well with the simulation results of the full non-linear equations of motion in terms of displacement, voltage, and power harvested. It is confirmed through analysis of the frequency transfer function that the non-linear system converges to the approximation by a series of free responses at low frequencies and to the linear system response at frequencies around the fundamental. Hence, a combination of analytical solutions can be used to predict the energy harvesting performance of this non-linear device in lieu of simulation of the full dynamics equations.

Author details

Adam Wickenheiser
George Washington University, United States

6. References

(1987). IEEE Standard on Piezoelectricity, IEEE, New York, NY.

Anderson, B. & Wickenheiser, A. (2012). Performance analysis of frequency up-converting energy harvesters for human locomotion. Proceedings of SPIE, ISSN 0277-786X.

Arrieta, A. F.; Hagedorn, P.; Erturk, A. & Inman, D. J. (2010). A piezoelectric bistable plate for nonlinear broadband energy harvesting. Applied Physics Letters, Vol. 97, 104102, ISSN 0003-6951.

Challa, V. R.; Prasad, M. G.; Shi, Y. & Fisher, F. T. (2008). A vibration energy harvesting device with bidirectional resonance frequency tenability. *Smart Materials and Structures*, Vol. 17, 015035, ISSN 0964-1726.

Davis, C. L. & Lesieutre, G. A. (1995). A modal strain energy approach to the prediction of resistively shunted piezoceramic damping. Journal of Sound and Vibration, Vol. 184, No. 1, pp. 129–139, ISSN 0022-460X.

Dietl, J. M. & Garcia, E. (2010). Beam shape optimization for power harvesting. Journal of Intelligent Material Systems and Structures, Vol. 21, pp. 633–646, ISSN 1045-389X.

duToit N. E., Wardle, B. L. & Kim, S. (2005). Design Considerations for MEMS-Scale Piezoelectric Mechanical Vibrations Energy Harvesting. Integrated Ferroelectrics, Vol.71, pp. 121–160, ISSN 1058-4587.

Erturk, A. & Inman, D. J. (2008). A Distributed Parameter Electromechanical Model for Cantilevered Piezoelectric Energy Harvesters. *Journal of Vibrations and Acoustics*, Vol. 130, No. 4, 041002, ISSN 1048-9002.

Erturk, A.; Renno, J. M. & Inman, D. J. (2009). Modeling of piezoelectric energy harvesting from an L-shaped beam-mass structure with an application to UAVs. Journal of Intelligent Materials Systems and Structures, Vol. 20, pp. 529–544, ISSN 1045-389X.

Inman, D. J. (2007). Engineering Vibration (3rd), Pearson, ISBN 0-13-228173-2, Upper Saddle River, NJ.

Karami, M. A. & Inman, D. J. (2011). Electromechanical Modeling of the Low-Frequency Zigzag Micro-Energy Harvester. Journal of Intelligent Material Systems and Structures, Vol. 22, No. 3, pp. 271–282, ISSN 1045-389X.

Lefeuvre, E.; Badel, A.; Benayad, A.; Lebrun, L.; Richard, C. & Guyomar, D. (2005). A comparison between several approaches of piezoelectric energy harvesting. Journal De Physique IV, Vol. 128, pp. 177–186, ISSN 1155-4339.

Leland, E. S. & Wright, P. K. (2006) Resonance tuning of piezoelectric vibration energy scavenging generators using compressive axial preload. Smart Materials and Structures, Vol. 15, No. 5, pp. 1413–20, ISSN 0964-1726.

Liao, Y. & Sodano, H. A. (2008). Model of a single mode energy harvester and properties for optimal power generation. Smart Materials and Structures, Vol. 17, No. 6, 065026, ISSN 0964-1726.

Lin, Y. K. (1967). Probabilistic Theory of Structural Dynamics, McGraw-Hill, ISBN 0-88-275377-0, New York, NY.

Mann, B. P. & Sims, N. D. (2009). Energy harvesting from the nonlinear oscillations of magnetic levitation, Journal of Sound and Vibration, Vol. 319, pp. 515-530, ISSN 0022-460X.

Moon, F. C. (1978). Problems in magneto-solid mechanics, Mechanics Today, Vol. 4, pp. 307-390.

Morris, D. J.; Youngsman, J. M.; Anderson, M. J. & Bahr, D. F. (2008). A resonant frequency tunable, extensional mode piezoelectric vibration harvesting mechanism, Smart Materials and Structures, Vol. 17, No. 6, 065021, ISSN 0964-1726.

Murray, R. & Rastegar, J. (2009). Novel Two-Stage Piezoelectric-Based Ocean Wave Energy Harvesters for Moored or Unmoored Buoys. Proceedings of SPIE, ISSN 0277-786X, San Diego, CA, March, 2009.

Oguamanam, D. C. D. (2003). Free vibration of beams with finite mass rigid tip load and flexural-torsional coupling. International Journal of Mechanical Sciences, Vol. 45, pp. 963–979, ISSN 0020-7403.

Porat, B. (1994). Digital Processing of Random Signals, Prentice-Hall, ISBN 0-48-646298-6, Englewood Cliffs, NJ.

Ramlan, R.; Brennan, M. J.; Mace, B. R. & Kovacic, I. (2010). Potential benefits of a non-linear stiffness in an energy harvesting device. Nonlinear Dynamics, Vol. 59, pp. 545–558, ISSN 0924-090X.

Rastegar, J. & Murray, R. (2008). Novel Two-Stage Electrical Energy Generators for Highly Variable and Low-Speed Linear or Rotary Input Motion. Proceedings of ASME, ISBN 9780791843260.

Reissman, T.; Dietl, J. M. & Garcia, E. (2007). Modeling and Experimental Verification of Geometry Effects on Piezoelectric Energy Harvesters. Proceedings of 3rd Annual Energy Harvesting Workshop, Santa Fe, NM, February, 2007.

Reissman T.; Wolff, E. M. & Garcia, E. (2009). Piezoelectric Resonance Shifting Using Tunable Nonlinear Stiffness. Proceedings of SPIE, Vol. 7288, 72880G–1, ISSN 0277-786X.

Roundy, S.; Leland, E. S.; Baker, J.; Carleton, E.; Reilly, E.; Lai, E.; Otis, B.; Rabaey, J.M.; Wright, P.K. & Sundararajan, V. (2005). Improving power output for vibration-based energy scavengers. Pervasive Computing, Vol. 4, No. 1, pp. 28–36, ISSN 1526-1268.

Roundy, S.; Wright, P. K. & Rabaey, J. (2003). A study of low level vibrations as a power source for wireless sensor nodes. Computer Communications, Vol. 26, No. 11, pp.1131–1144, ISSN 0140-3664.

Shu, Y. C. & Lien, I. C. (2006). Analysis of power output for piezoelectric energy harvesting systems. Smart Materials and Structures, Vol. 15, No. 6, pp. 1499–1512, ISSN 0964-1726.

Sodano, H. A., Park, G. & Inman, D. J. (2004). Estimation of Electric Charge Output for Piezoelectric Energy Harvesting. *Strain*, Vol. 40, No. 2, pp. 49–58, ISSN 0039-2103.

Söderkvist, J. (1990). Electric Equivalent Circuit for Flexural Vibrations in Piezoelectric Materials. IEEE Transactions on Ultrasonics, Ferroelectrics, and Frequency Control, Vol. 37, No. 6, pp. 577–586, ISSN 0885-3010.

Stanton, S. C., McGehee, C. C., & Mann, B. P. (2010). Nonlinear Dynamics for Broadband Energy Harvesting: Investigation of A Bistable Piezoelectric Inertial Generator. Physica D, Vol. 239, pp. 640–653, ISSN 0167-2789.

Tieck, R. M.; Carman, G. P. & Lee, D. G. E. (2006). Electrical Energy Harvesting Using a Mechanical Rectification Approach. Proceedings of IMECE, pp. 547–553, ISBN 0-79-183790-4.

Wickenheiser, A. M. (2011). Design Optimization of Linear and Nonlinear Cantilevered Energy Harvesters for Broadband Vibrations. Journal of Intelligent Material Systems and Structures, Vol. 22, pp. 1213–1225, ISSN 1045-389X.

Wickenheiser, A. M. (2012). Eigensolution of piezoelectric energy harvesters with geometric discontinuities: Analytical modeling and validation. Journal of Intelligent Material Systems and Structures, published online, ISSN 1045-389X.

Wickenheiser, A. & Garcia, E. (2010a). Design of energy harvesting systems for harnessing vibrational motion from human and vehicular motion. Proceedings of SPIE, ISSN 0277-786X, San Diego, CA, March, 2010.

Wickenheiser, A. M. & Garcia, E., (2010b). Broadband vibration-based energy harvesting improvement through frequency up-conversion by magnetic excitation. *Smart Materials and Structures*, Vol. 19, No. 6, 065020, ISSN 0964-1726.

Wickenheiser, A. M. & Garcia, E. (2010c). Power Optimization of Vibration Energy Harvesters Utilizing Passive and Active Circuits. Journal of Intelligent Materials Systems and Structures, Vol. 21, No. 13, pp. 1343–1361, ISSN 1045-389X.

IntechOpen